JCTC Journal of Chemical Theory and Computation

Article

pubs.acs.org/JCTC

Serial Generalized Ensemble Simulations of Biomolecules with Self-Consistent Determination of Weights

Riccardo Chelli*[,†,‡] and Giorgio F. Signorini[†]

[†]Dipartimento di Chimica, Università di Firenze, Via della Lastruccia 3, I-50019 Sesto Fiorentino, Italy

[‡]European Laboratory for Nonlinear Spectroscopy (LENS), Via Nello Carrara 1, I-50019 Sesto Fiorentino, Italy

Supporting Information

ABSTRACT: Serial generalized ensemble simulations, such as simulated tempering, enhance phase space sampling through non-Boltzmann weighting protocols. The most critical aspect of these methods with respect to the popular replica exchange schemes is the difficulty in determining the weight factors which enter the criterion for accepting replica transitions between different ensembles. Recently, a method, called BAR-SGE, was proposed for estimating optimal weight factors by resorting to a self-consistent procedure applied during the simulation (*J. Chem. Theory Comput.* **2010**, *6*, 1935−1950). Calculations on model systems have shown that BAR-SGE outperforms other approaches proposed for determining optimal weights in serial generalized ensemble simulations. However, extensive tests on real systems and on convergence features with respect to the replica exchange method are lacking. Here, we report on a thorough analysis of BAR-SGE by performing molecular dynamics simulations of a solvated alanine dipeptide, a system often used as a benchmark to test new computational methodologies, and comparing results to the replica exchange method. To this aim, we have supplemented the ORAC program, a FORTRAN suite for molecular dynamics simulations (*J. Comput. Chem.* **2010**, *31*, 1106−1116), with several variants of the BAR-SGE technique. An illustration of the specific BAR-SGE algorithms implemented in the ORAC program is also provided.

1. INTRODUCTION

Generalized ensemble methods[1] are commonly used in computer simulations of systems with a complex free energy landscape to estimate thermodynamic averages through non-Boltzmann phase space sampling. For example, in simulated tempering[2,3] and temperature Replica Exchange[4−7] (RE), a random walk in temperature space allows the system to overcome energy barriers much larger than k_BT and hence to explore important phase space regions that are difficult to sample with conventional simulations. In both methods, copies of the system (replicas) are allowed to move in a generalized phase space, defined by the usual dynamical variables (atomic coordinates and momenta), plus a discretized variable (denoted as λ in the following) that represents different temperatures. Standard equations of motion are employed to evolve atomic positions and momenta, while a Monte Carlo-like algorithm is used to perform temperature transitions of the replicas via λ changes. More generally, as it occurs in Hamiltonian RE[8,9] and solute tempering,[10−12] λ is a parameter entering the Hamiltonian of the system, and transitions occur between ensembles with different values of λ. In all generalized ensemble methods, the configurations of all replicas can be exploited *a posteriori* to calculate thermal averages, using reweighting techniques.[13−15]

The classification of *Serial* Generalized Ensemble (SGE) and *Parallel* Generalized Ensemble (PGE) algorithms is sometimes used to distinguish between schemes based on single-replica transitions (like in simulated tempering) and those based on swaps of replica pairs (like in RE), respectively.[16] Comparisons between SGE and PGE methods have been reported.[17−19] The overall conclusions of these studies are that SGE methods consistently give a higher rate of delivering the system between ensembles with large and small λ values (low and high temperature states in simulated tempering), as well as a higher rate of transversing the potential energy space. Moreover, SGE methods are well-suited to distributed computing environments because they do not need the synchronization of all processes that is instead required by standard PGE schemes (with the exception of the asynchronous versions of RE[20]). On the other side, in order to get uniform sampling of the ensembles in SGE simulations, one has to apply weight factors equal to the free energies of the λ ensembles. The knowledge of such free energies is not needed in PGE methods because replica exchanges do not imply free energy variations. Determination of free energies of λ ensembles is the most critical aspect of SGE schemes. In fact, as remarked in ref 17, the estimate of accurate weight factors may be very difficult for complex systems. Inaccurate estimates, though not affecting the basic principles of SGE methods, do affect the sampling performances in terms of simulation time needed to achieve convergence of structural properties.[17] This issue has been the subject of many studies, especially addressed to simulated tempering simulations.[3,16,18,21−25]

Recently, a self-consistent method to calculate optimal weights in SGE simulations has been proposed.[26] This method, called BAR-SGE, gives asymptotically exact results and is based on generalized expressions[27,28] of the Bennett acceptance ratio[29] and free energy perturbation.[30] It has been shown that its accuracy is comparable to the multiple-histogram reweighting approach,[13,14] with a modest additional computing time with respect to a conventional simulation. BAR-SGE was applied to a simple model system,[26] where it was shown to outperform other computational strategies for determining optimal weights.[16,25] However, the actual performances of BAR-SGE with respect to

Received: November 23, 2011
Published: January 24, 2012

   dx.doi.org/10.1021/ct2008457 | *J. Chem. Theory Comput.* 2012, 8, 830−842

the popular RE have not yet been investigated. In this article, we present the results on two BAR-SGE simulations (with one and eight replicas) and one RE simulation (with eight replicas) related to a physically sound system, i.e., an alanine dipeptide in water solution. As we will see, this system is quite challenging because a canonical simulation at room temperature is unable to fully explore the free energy surface in terms of the Φ and Ψ dihedral angles (Figure 1). For this reason, the alanine dipeptide has been taken often as a benchmark to verify new computational methodologies for exploring free energy surfaces.[9,31,32] The BAR-SGE technique has been implemented in the open-source molecular dynamics simulation program ORAC.[33,34] In particular, we have supplemented the program with a module that allows the user to perform (i) simulated tempering based on Hamiltonian scaling,[8] (ii) simulated solute tempering,[12] and (iii) an SGE variant of multiple-window umbrella sampling[35,36] on user-defined internal coordinates such as interatomic distances and bending and dihedral angles. The ORAC program is distributed free of charge under the GNU general public license (GPL) at http://www.chim.unifi.it/orac.

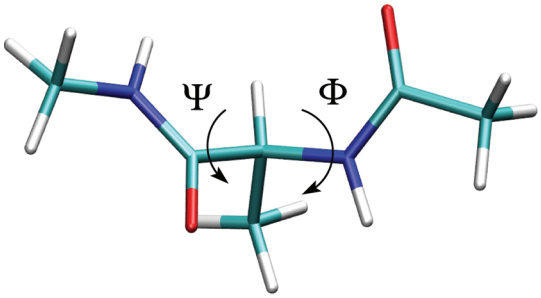

Figure 1. Representation of the Φ and Ψ angles in alanine dipeptide.

The outline of the article follows. In section 2, we define the acronyms used throughout the article along with the definitions of few widely employed terms/abbreviations. In section 3, we introduce the SGE theory. The implementation of several SGE variants in the ORAC program is illustrated in section 4, while the BAR-SGE algorithm is described in section 5. Details on the simulations and on the system are presented in section 6. In section 7, we report and discuss the results of the simulations. Concluding remarks can be found in section 8.

2. GLOSSARY AND ACRONYMS

BAR-SGE method: method based on the Bennett Acceptance Ratio to update optimal weights in serial generalized ensemble simulations.
MBAR: Multistate Bennett Acceptance Ratio.
Multiensemble methods/simulations/techniques: alternative term employed to indicate both serial and parallel generalized ensemble methods/simulations/techniques.
MWT: MultiWindow Tempering.
Optimal weights: alternative term employed to denote the dimensionless free energies of the λ ensembles.
PGE: Parallel Generalized Ensemble.
RE: Replica Exchange.
Replica: a "copy" of the simulated system (or simulation walker) running through the λ ensembles.
Replica transition: a jump of a replica from the current λ ensemble to a neighboring one, i.e., from a λ_n ensemble to a λ_{n+1} (or λ_{n-1}) ensemble.
SGE: Serial Generalized Ensemble.
SGE-1 simulation: serial generalized ensemble simulation based on the BAR-SGE method and realized with one replica.
SGE-8 simulation: serial generalized ensemble simulation based on the BAR-SGE method and realized with eight replicas.
SST: Simulated Solute Tempering.
λ ensemble: a λ-dependent ensemble in the context of serial and parallel generalized ensemble methods.

3. THEORETICAL BACKGROUND: SERIAL GENERALIZED ENSEMBLE METHOD

In SGE molecular dynamics simulations, one or more copies of the system (replicas) realize independent trajectories in an extended phase space. This phase space includes the usual atomic coordinates and momenta (from now on denoted as x and p, respectively) and a discretized variable associated with thermodynamic ensembles which may have different Hamiltonians as well. The evolution of the replicas in the (x,p) subspace occurs as in conventional molecular dynamics simulations, while the "motion" in the space of the additional variable, which practically corresponds to a path through the various ensembles, is realized in a Monte Carlo fashion. In this section, we illustrate the general principles of the SGE method and derive the expression for the basic quantity, namely the probability of accepting a replica jump from one ensemble to another.

Let us indicate a generic dimensionless Hamiltonian associated with the nth ensemble as $h_n(x,p)$,[37] where $n \in (1, 2, ..., N)$, with N being the (finite) number of ensembles. The partition function of the nth ensemble is

$$Z_n = \int_\Gamma e^{-h_n(x,p)}\, dx\, dp \tag{1}$$

where Γ indicates that the domain of integration is the whole (x,p) phase space. In simulated tempering simulations, the dimensionless Hamiltonian is $h_n(x,p) = \beta_n H(x,p)$, where $H(x,p)$ is the physical Hamiltonian and $\beta_n = (k_B T_n)^{-1}$, k_B being the Boltzmann constant and T_n the temperature of ensemble n. If, on the other hand, all ensembles have the same temperature, but the Hamiltonian of ensemble n is expressed parametrically through the variable λ_n, then the dimensionless Hamiltonian can be written as

$$h_n(x, p) = \beta H(x, p; \lambda_n) \tag{2}$$

There is large freedom in choosing the λ-dependence of the Hamiltonian. The variable can simply scale some potential energy term or be correlated with an arbitrary collective coordinate of the system through an additional potential term, or even correspond to the pressure. It is also possible to construct a generalized ensemble for many parametric variables,[38] but such a possibility will not be addressed here. Multiensemble algorithms have a different implementation depending on whether the temperature is included in the collection of the parametric variables or not. Here, we adhere to the most general context without specifying any form of $h_n(x,p)$, thus deriving a general expression for the acceptance probability. The specific algorithms supplied with the ORAC program will be illustrated in section 4. In SGE simulations, the probability of a microstate (x,p) in the nth ensemble (from now on denoted as $(x,p)_n$) is proportional to $\exp[-h_n(x,p) + g_n]$, where g_n is a weight factor defined for each ensemble $n \in (1, 2, ..., N)$.

dx.doi.org/10.1021/ct2008457 | J. Chem. Theory Comput. 2012, 8, 830−842

The partition function of the extended ensemble described by x, p, and λ_n is

$$Z = \sum_{n=1}^{N} \int_{\Gamma} e^{-h_n(x,p)+g_n} \, dx \, dp = \sum_{n=1}^{N} Z_n \, e^{g_n} \tag{3}$$

where Z_n is the partition function of the system in the nth ensemble (eq 1).

In practice, SGE simulations work as follows. A single simulation is started in a specific ensemble using a molecular dynamics scheme, and at (not necessarily) regular time intervals, attempts are made to change the current microstate, say $(x,p)_n$, to another microstate of a different ensemble, $(x',p')_m$. Since acceptance rates are correlated to the overlap between ensembles, the final ensemble m is typically chosen close to the initial one, namely, $m = n \pm 1$.[39] In principle, the initial and final microstates can be defined by different coordinates and/or momenta ($x \neq x'$ and/or $p \neq p'$), though the condition $x = x'$ is usually adopted. Moreover, in conventional simulated tempering simulations, when a replica transition is accepted, it is common practice to rescale the atomic momenta to the target temperature[26] ($p \neq p'$). We point out that such a rescaling is not strictly necessary; however, it is useful because it increases the acceptance probability of the transition by making it possible to eliminate the kinetic energy from the acceptance ratio (eq 6 below). By contrast, when temperature is constant across ensembles (eq 2), as in our implementation of SGE, no rescaling of momenta is needed: $x = x'$ and $p = p'$. The probabilities of conjugated replica transitions, $(x,p)_n \rightarrow (x,p)_m$ and $(x,p)_m \rightarrow (x,p)_n$, must satisfy the detailed balance condition:

$$P_n(x, p) \, P(n \rightarrow m) = P_m(x, p) \, P(m \rightarrow n) \tag{4}$$

where $P_n(x,p)$ is the probability of the microstate $(x,p)_n$ in the extended ensemble (whose partition function is that of eq 3):

$$P_n(x, p) = Z^{-1} \, e^{-h_n(x,p)+g_n} \tag{5}$$

In eq 4, $P(n \rightarrow m)$ is shorthand for the conditional probability of the transition $(x,p)_n \rightarrow (x,p)_m$ to happen given the system is in the microstate $(x,p)_n$ (with analogous meaning of $P(m \rightarrow n)$). Using eq 5 together with the analogous expression for $P_m(x,p)$ in the detailed balance and applying Metropolis's criterion, we find that the transition $(x,p)_n \rightarrow (x,p)_m$ is accepted with probability

$$\mathrm{acc}[n \rightarrow m] = \min(1, \, e^{h_n(x,p)-h_m(x,p)+g_m-g_n}) \tag{6}$$

Note that, according to Metropolis, the above expression holds only if the transition $(x,p)_n \rightarrow (x,p)_m$ and its conjugated $(x,p)_m \rightarrow (x,p)_n$ are attempted with the same probability. Usually, upward and downward replica transitions ($(x,p)_n \rightarrow (x,p)_{n+1}$ and $(x,p)_n \rightarrow (x,p)_{n-1}$, respectively) are picked with probability equal to 0.5. The probability of sampling a given ensemble is

$$P_n = \int_{\Gamma} P_n(x, p) dx \, dp = Z_n Z^{-1} e^{g_n} \tag{7}$$

Uniform sampling sets the condition $P_n = N^{-1}$ for each ensemble, which leads to the equality

$$g_n = -\ln Z_n + \ln\left(\frac{Z}{N}\right) \tag{8}$$

Equation 8 implies that, to get uniform sampling of the ensembles, the difference $g_m - g_n$ in eq 6 must be replaced with $f_m - f_n$ (from now on denoted as $\Delta f_{n \rightarrow m}$), where f_n is the dimensionless free energy related to the actual free energy of the ensemble n by the relation $f_n = \beta F_n = -\ln Z_n$, where β is the inverse temperature of the ensembles. BAR-SGE is a method to determine the f_n free energies, also referred to here as optimal weights.

4. IMPLEMENTATIONS OF THE SERIAL GENERALIZED ENSEMBLE METHOD (IN THE ORAC PROGRAM)

4.1. Simulated Solute Tempering. The ability of simulated tempering[2,3] to overcome free energy barriers arises from the fact that the free energy surface becomes flatter as the temperature increases or, in other words, that the dynamics of the system becomes insensitive to the roughness of the potential energy with increasing temperature. The same effect can therefore be obtained by scaling the potential energy of the system by some positive factor smaller than one and keeping the temperature fixed. The smaller the factor, the higher the virtual temperature of the replica. Such a strategy is exploited, for example, in the Hamiltonian RE method,[8,9,34] where different replicas are characterized by different interatomic interactions rather than by different temperatures.

Therefore, following the idea first proposed by Li et al.,[12] the ORAC program has been supplemented by the possibility of applying tempering to different parts of the potential energy, allowing the scaling of specific types of interactions (e.g., solute−solute and solute−solvent interactions rather than solvent−solvent interactions). The adopted approach is similar to the simulated solute tempering (SST) proposed by Denschlag et al.,[11] that was, in turn, inspired by RE solute tempering of Liu et al.[10] However, unlike standard implementations of solute tempering, the "solute" can be any *segment* of the system, generically intended as a subset of atoms, not necessarily correlated in space. The definition of segment is in principle arbitrary, but good choices should account for the portions of system strongly coupled to the relevant coordinates for the process under study. This allows one to minimize the number of degrees of freedom involved in replica transitions and, hence, the number of λ ensembles for a given λ range.[12] As a result, the average time for delivering a replica from the lowest to the highest λ value and vice versa (round-trip time) is substantially reduced. Another significant difference with Denschlag's[11] SST implementation, is that in our approach a replica transition does not imply a temperature change but rather a potential energy scaling.

The algorithm works as follows. We define the *segment* as a subset of atoms of the system that may include disconnected portions of the solute and selected solvent molecules as well; the remaining atoms define the *environment* around the segment. The global potential energy, $V(x)$, can be partitioned as

$$V(x) = V_{ss}(x) + V_{se}(x) + V_{ee}(x) + v_{qr}(x) \tag{9}$$

where $V_{ss}(x)$, $V_{se}(x)$, and $V_{ee}(x)$ include the segment−segment, segment−environment, and environment−environment interactions, respectively, stripped of the reciprocal lattice electrostatic energy, $v_{qr}(x)$. The partitioning of $v_{qr}(x)$ is not realized because, in the particle mesh Ewald approach[40,41] employed in ORAC,[33] segment−segment, segment−environment, and environment−environment contributions to $v_{qr}(x)$ cannot be separated. As we will see, the potential energy partitioning of eq 9 allows one to leave $v_{qr}(x)$ out of energy scaling in replica transitions. From the sampling standpoint, this is however irrelevant, because $v_{qr}(x)$ is a long-range potential, and thus it is

dx.doi.org/10.1021/ct2008457 | J. Chem. Theory Comput. 2012, 8, 830−842

rather insensitive to structural variations with respect to the short-range energy components.

A further partitioning of $V_{ss}(x)$, $V_{se}(x)$, and $V_{ee}(x)$ is also done on the basis of the different kinds of intra- and intermolecular potential energy terms. In particular, we split these potential energies according to the following physically justified subdivision:

$$\begin{aligned} v_1^\alpha(x) &= v_{str}^\alpha(x) + v_{ben}^\alpha(x) + v_{ito}^\alpha(x) \\ v_2^\alpha(x) &= v_{pto}^\alpha(x) + v_{14}^\alpha(x) \\ v_3^\alpha(x) &= v_{lj}^\alpha(x) + v_{qd}^\alpha(x) \end{aligned} \tag{10}$$

where α denotes the type of interacting portions of the system (ss, se, or ee). The first potential energy term collects all contributions that generate "fast" motions: stretching, $v_{str}^\alpha(x)$; bending, $v_{ben}^\alpha(x)$; and improper torsional interactions, $v_{ito}^\alpha(x)$. The second term collects the proper torsional interactions, $v_{pto}^\alpha(x)$, and the so-called 1−4 interactions, $v_{14}^\alpha(x)$. The third term collects all of the nonbonded interactions, namely, the Lennard-Jones energy, $v_{lj}^\alpha(x)$, and the direct lattice electrostatic energy, $v_{qd}^\alpha(x)$. We refer to ref 33 (eqs 4−13) for a complete discussion of the interaction potential energies and of the detailed meaning of the symbols in eq 10. Thus, the potential energies $V_{ss}(x)$, $V_{se}(x)$, and $V_{ee}(x)$ can be represented by vectors whose components are in eq 10. For example, $\mathbf{v}_{se}(x) \equiv (v_1^{se}(x),v_2^{se}(x),v_3^{se}(x))$, with $V_{se}(x) = v_1^{se}(x) + v_2^{se}(x) + v_3^{se}(x)$. Using such notation, we propose the following expression for the dimensionless Hamiltonian of a replica in ensemble n:

$$\begin{aligned} h_n(x, p) = \beta[&\boldsymbol{\lambda}_n^{ss}\cdot\mathbf{v}_{ss}(x) + \boldsymbol{\lambda}_n^{se}\cdot\mathbf{v}_{se}(x) + V_{ee}(x) \\ &+ v_{qr}(x) + u(p)] \end{aligned} \tag{11}$$

where $u(p)$ is the kinetic energy of the system, dependent on the atomic momenta p. In molecular dynamics simulations, $u(p)$ may include additional energy contributions dependent on variables specific to the adopted thermodynamic environment (constant-(p,T) ensembles, constant-(V,T) ensembles, etc.). For instance, if constant-(p,T) simulations are carried out, then $u(p)$ also includes the energies needed for keeping constant both pressure and temperature (the pV term and the kinetic energies of thermostat and barostat[42]). The vectors $\boldsymbol{\lambda}_n^{ss}$ and $\boldsymbol{\lambda}_n^{se}$ account for independent changes of the intra- and intermolecular energy contributions in replica transitions (eq 10). Like in solute tempering schemes, the environment−environment interactions are constant across ensembles. Note that the original dimensionless Hamiltonian is associated with the ensemble for which the relation $\boldsymbol{\lambda}_n^{ss} = \boldsymbol{\lambda}_n^{se} = (1, 1, ...,1)$ holds. In eq 11, $V_{ee}(x)$, $v_{qr}(x)$, and $u(p)$ do not change in replica transitions and therefore do not affect the acceptance probability. The acceptance probability for an attempted $(x,p)_n \rightarrow (x,p)_m$ transition is obtained by substituting eq 11 into eq 6 and assuming $g_n = f_n$ in the latter:

$$\begin{aligned} &\mathrm{acc}[n \rightarrow m] \\ &\quad = \min(1, e^{\beta[(\boldsymbol{\lambda}_n^{ss}-\boldsymbol{\lambda}_m^{ss})\cdot\mathbf{v}_{ss}(x)+(\boldsymbol{\lambda}_n^{se}-\boldsymbol{\lambda}_m^{se})\cdot\mathbf{v}_{se}(x)]+\Delta f_{n\rightarrow m}}) \end{aligned} \tag{12}$$

where $\Delta f_{n\rightarrow m} = f_m - f_n$.

From the point of view of a molecular dynamics simulation, the advantage of using our SST approach with respect to conventional simulated tempering or the SST proposed in ref 11 is two-fold. First, as a replica has the same operating temperature in all λ ensembles, one does not have to rescale the atomic momenta after a successful replica transition. Second, since the mean atomic velocities are the same throughout the extended system, one does not have to adapt the simulation time-step for preserving the quality of the integrator, as it should be done instead when using other methods. In the ORAC SST implementation, one or more replicas may run independently, apart from when replicas exchange information to update the optimal weights (see discussion in section 5). Each replica is thus associated with a different CPU process of a parallel simulation. When a CPU process periodically writes out the atomic coordinates of the corresponding replica (typically in *pdb* or *xyz* format), one must also keep track of the vectors $\mathbf{v}_{ss}(x)$, $\mathbf{v}_{se}(x)$, $\boldsymbol{\lambda}_n^{ss}$, and $\boldsymbol{\lambda}_n^{se}$ (the program does this automatically) to apply a reweighting analysis[13−15] to configurations sampled at thermodynamical conditions different from the target one.

In principle there are not strong limitations in setting $\boldsymbol{\lambda}_n^\alpha$. However, a typical choice is to set the components related to $v_1^\alpha(x)$ (see eq 10) equal to 1 for all of the ensembles. In fact, there is little advantage for conformational sampling in softening degrees of freedom that do not contribute to the molecular flexibility. With this choice, these interactions do not enter the acceptance probability of eq 12, and a further lowering of the degrees of freedom is gained. On the other hand, conformational transitions are mainly driven by torsional and nonbonded interactions, so it becomes convenient to "heat up" these degrees of freedom by scaling the corresponding potential functions.

Obviously, molecular dynamics simulations can also be performed without defining any segment in the simulated system. In such a case, a sort of Hamiltonian tempering[8,9] is realized, where scaling is applied to the whole potential energy. The dimensionless Hamiltonian of a replica in ensemble n is written as

$$h_n(x, p) = \beta[\boldsymbol{\lambda}_n\cdot\mathbf{v}(x) + u(p)] \tag{13}$$

where $u(p)$ has the usual meaning. In eq 13, the whole potential energy $V(x)$ is partitioned as in eq 10 and is thus represented by the vector $\mathbf{v}(x) \equiv (v_1(x),v_2(x),v_3(x))$, with $v_{qr}(x)$ being included into $v_3(x)$. The acceptance probability for an attempted $(x,p)_n \rightarrow (x,p)_m$ replica transition is easily obtained substituting eq 13 into eq 6. Given the similarity with Hamiltonian RE,[8,9] we term this approach *Hamiltonian simulated tempering*.

4.2. Multiwindow Tempering. A further interesting feature of ORAC is the possibility of performing SGE simulations based on multiple-window umbrella sampling.[35,36] In multiple-window umbrella sampling, the sampling is realized in the space of a user-defined collective coordinate through the addition of constraining potential energy terms, called window potentials, to the Hamiltonian of the system. The method was originally devised to perform a number of *independent* simulations of copies of the system with Hamiltonians supplemented with different window potentials. Therefore, each simulation forces the system to visit configurational states characterized by different values of the collective coordinate. At the end of the simulations, it is possible to calculate the potential of mean force along the collective coordinate and, in general, any other equilibrium quantity using weighted histogram analysis methods.[13−15]

The extension of multiple-window umbrella sampling to the framework of SGE simulations is straightforward.

dx.doi.org/10.1021/ct2008457 | J. Chem. Theory Comput. 2012, 8, 830−842

Each ensemble corresponds to a given window potential. The trajectory of a replica is started in one ensemble; then, at established time intervals, transitions of the replica toward a neighboring ensemble are attempted. Because of the peculiarity of replicas to move through ensembles with different window potentials, we term this approach *MultiWindow Tempering* (MWT). A description of the method is reported in Appendix A.

Note: thermodynamic expectations in SST and MWT are calculated via multistate Bennett acceptance ratio analysis[15] (MBAR). The basic equations of MBAR are given in section I of the Supporting Information.

5. CALCULATION OF OPTIMAL WEIGHTS

In this section, we report the basic equations needed to calculate the optimal weights via BAR-SGE and a description of the self-consistent algorithm. A more detailed discussion can be found in ref 26.

In SGE simulations, the main quantity to be calculated is the acceptance probability of eq 6. In order to simplify the notation in the following discussion, we rewrite eq 6 as

$$\mathrm{acc}[n \to m] = \min(1, \mathrm{e}^{-W[n\to m]+\Delta f_{n\to m}}) \tag{14}$$

where $W[n \to m] = h_m(x,p) - h_n(x,p)$ can be interpreted as the generalized dimensionless work done on the system in the $(x,p)_n \to (x,p)_m$ transformation.[26,28] The specific expressions of $W[n \to m]$ for the SST and MWT are easily recovered from the results of section 4.1 and Appendix A, respectively. The important aspect of the procedure is that the knowledge of $W[n \to m]$ and $W[m \to n]$ stored for each replica during the simulation allows us to evaluate $\Delta f_{n\to m}$. Thus, for each pair of neighboring ensembles n and m, we generate two collections of "instantaneous dimensionless work" elements: $W_1[m \to n]$, $W_2[m \to n]$, ..., etc. and $W_1[n \to m]$, $W_2[n \to m]$, ..., etc. Indicating the number of elements with $N_{m\to n}$ and $N_{n\to m}$, we can find $\Delta f_{n\to m}$ by solving the equation[26,28,43]

$$\sum_{i=1}^{N_{n\to m}} \left[1 + \frac{N_{n\to m}}{N_{m\to n}} \mathrm{e}^{W_i[n\to m]-\Delta f_{n\to m}}\right]^{-1} - \sum_{j=1}^{N_{m\to n}} \left[1 + \frac{N_{m\to n}}{N_{n\to m}} \mathrm{e}^{W_j[m\to n]+\Delta f_{n\to m}}\right]^{-1} = 0 \tag{15}$$

which corresponds to the Bennett acceptance ratio[29] for dimensionless quantities. It is clear that to employ eq 15, both n and m ensembles must be visited at least once. If statistics are instead retrieved from one ensemble alone, say n, then we must resort to a different approach. In the limit that only one work collection (say, the $n \to m$ collection) is available, eq 15 becomes[43]

$$\mathrm{e}^{-\Delta f_{n\to m}} = N_{n\to m}^{-1} \sum_{i=1}^{N_{n\to m}} \mathrm{e}^{-W_i[n\to m]} \tag{16}$$

In this equation, we recognize the popular Zwanzig formula for free energy perturbation[30] and the Jarzynski equality[44] for instantaneous realizations.

In an SGE simulation realized in a space of N ensembles, the $\Delta f_{1\to 2}$, $\Delta f_{2\to 3}$, ..., $\Delta f_{N-1\to N}$ quantities have to be estimated. The protocol can be summarized in a few points.

(1) At the beginning of the simulation, the replica is assigned to a randomly chosen ensemble, and the sampling starts with the established molecular dynamics protocol. For the sake of simplicity, here we will describe the algorithm for only one replica, leaving the discussion of multiple-replica simulations to the final part of this section.

(2) When the replica is in ensemble n, the work samples $W[n \to n+1]$ and $W[n \to n-1]$ are stored into CPU memory, and the numbers of stored samples, $N_{n\to n+1}$ and $N_{n\to n-1}$, are updated. These operations are accomplished every L_a steps, taking some care in storing work samples that are uncorrelated. This is because, while correlated work values do not improve significantly the accuracy of free energy estimates via eq 15, a large number of work samples (i.e., large $N_{n\to m}$ values) raises their computational cost.

(3) Every L_b steps, such that L_b is at least 2 or 3 orders of magnitude greater than L_a, a free energy estimate is attempted on the basis of eq 15 or eq 16. The scheme adopted for a generic $\Delta f_{n\to n+1}$ follows.

(3a) First, we check if both conditions $N_{n\to n+1} > N'$ and $N_{n+1\to n} > N'$ are met. In such a case, eq 15 is applied using the stored dimensionless works (see point 2). The threshold N' is used as a control parameter for the accuracy of the calculation. Note that this estimate of $\Delta f_{n\to n+1}$ is not used as such in the acceptance probability of eq 14. Rather, it is employed to update the actual optimal weight applying standard formulas from maximum likelihood considerations, as described in Appendix B. After updating the optimal weight from eq 25, we reset $N_{n\to n+1}$, $N_{n+1\to n}$, $W[n \to n+1]$, and $W[n+1 \to n]$ for the next independent estimate of $\Delta f_{n\to n+1}$. This step is realized for each $n \in (1, 2, ..., N-1)$.

(3b) If the criteria needed to apply eq 15 are not met and no optimal weight is still available from eq 25 (see point 3a), then we try to apply eq 16. In such a case, the resulting free energy difference is used directly as the optimal weight in the acceptance probability. In particular, two independent estimates are attempted: one employed in the acceptance probability of upward replica transitions, $\Delta f_{n\to n+1}$, and the other employed for downward transitions, $\Delta f_{n+1\to n}$ (see next point 4). However, in order to apply eq 16 for estimating $\Delta f_{n\to n+1}$ and $\Delta f_{n+1\to n}$, the conditions $N_{n\to n+1} > N'$ and $N_{n+1\to n} > N'$ must, in turn, be satisfied. We stress again that this procedure is only targeted to furnish a reliable evaluation of optimal weights when they are still not available from the bidirectional algorithm illustrated at point 3a.

(3c) If none of the above criteria is met, then the optimal weight is not updated and conventional sampling continues. Storage of dimensionless works as described in point 2 continues as well.

(4) Every L_c steps, a transition $(x,p)_n \to (x,p)_{n\pm 1}$ is attempted on the basis of the acceptance probability of eq 14. If the optimal weight for the chosen upward/downward transition is still not available from the methods described in points 3a and 3b, then the transition is not realized. The probabilities of generating upward and downward replica transitions are 0.5.

dx.doi.org/10.1021/ct2008457 | J. Chem. Theory Comput. 2012, 8, 830−842

In principle, the number M of running replicas can vary from one to infinity. However the best computational performance can be obtained enforcing a one-to-one correspondence between replicas and computing processors. A rough parallelization could be obtained performing M independent single-replica SGE simulations and then drawing the final data from all replicas to get augmented statistics. However, the calculation of the optimal weights would be much improved if they were periodically updated during the simulation on the basis of the data drawn on the fly from all replicas. This is just what ORAC does. In this respect, we remark that the multiple-replica BAR-SGE algorithm is prone to work efficiently also in distributed computing environments. The phase of the simulation where information is exchanged is the one described in the above point 3. It must be noted that, when an optimal weight update is performed, the stored work arrays (see point 2) do not need to be communicated among the replicas/processors. The sums appearing in eqs 15, 16, and 24 are perfectly parallelizeable in an MPI environment (like in ORAC). The computational cost arising from computer communications is further reduced because optimal weights can be updated rarely. Furthermore, in order to speed up the convergence, the initial distribution of the M replicas throughout the λ ensembles is roughly uniform, namely replica 1 in the λ_1 ensemble, replica 2 in the λ_2 ensemble, and so on.

6. SIMULATIONS AND SYSTEM

The system is made of one alanine dipeptide molecule (Figure 1) and 288 water molecules. The dipeptide is modeled using the AMBER03 force field,[45] while the TIP3P model[46] is used for water. Lorentz−Berthelot mixing rules are employed to account for the Lennard-Jones interactions between different kinds of atoms. Four simulations have been carried out: one RE simulation with eight replicas, two SGE simulations with one and eight replicas (denoted as SGE-1 and SGE-8 in the following), and one conventional canonical simulation. All simulations are realized in the constant-(V,T) thermodynamic ensemble adopting a cubic box with 21 Å side-lengths with standard periodic boundary conditions. The temperature control (298 K) is achieved using a Nosé−Hoover thermostat.[47] Electrostatic forces are treated with the smooth particle mesh Ewald method[41] using a fourth order B-spline interpolation polynomial for the charges,[33] an Ewald parameter of 0.43 Å^{-1}, and a grid spacing of 0.875 Å for the fast Fourier transform calculation of the charge weighted structure factor. The cutoff distance for the nonbonded interactions is 9.5 Å. A five time-step r-RESPA integrator,[48] as described in ref 33, is employed for integrating the equations of motion (with a largest time step of 6 fs). The initial system configuration is generated by placing the alanine dipeptide ($\Phi = -45.7°$ and $\Psi = 152.7°$) in the simulation box together with 288 water molecules arranged in a cubic lattice. Care has been taken to prevent overlap between dipeptide and water molecules. The equilibration phase (the period of time with no data storing) is very short: 3 ps with atomic velocity scaling followed by 3 ps of free system evolution. The equilibration period has been taken to be intentionally short, to enforce conditions unfavorable to BAR-SGE and to see how it works when optimal weights are still inaccurate. In fact, BAR-SGE is known to suffer from some difficulty at the beginning of the simulation.[26] In these stages, the lack of accurate optimal weights makes the walk of replicas in λ space highly unreliable (this aspect will be discussed in section 7). This inaccuracy clearly affects the thermodynamical averages in the first part of the production run. However, as optimal weights reach a smooth time-dependent regime thanks to the onset of the bidirectional algorithm (see point 3a in section 5), this negative effect is going to be leveled off.

The two SGE simulations have been performed using the SST method described in section 4.1. The same method[34] has been used for the RE simulation. In particular, the algorithm with equal segment−segment and segment−environment scaling is applied ($\boldsymbol{\lambda}_n^{ss} = \boldsymbol{\lambda}_n^{se} = \boldsymbol{\lambda}_n$), the segment being defined by the 22 atoms of the alanine dipeptide (see eq 11 and 12 for the expressions of the Hamiltonian and the acceptance probability). Eight ensembles are included in the simulations, whose associated $\boldsymbol{\lambda}_n$ vectors are reported in Table 1. In the following section, we will denote a specific λ ensemble with the corresponding vector $\boldsymbol{\lambda}_n$. Note that, within each ensemble, the scaling parameters for the $v_{pto}(x)$, $v_{14}(x)$, $v_{lj}(x)$, and $v_{qd}(x)$ potential energy terms ($\lambda_n^{(2)}$ and $\lambda_n^{(3)}$ in Table 1) have been arbitrarily set to be equal. As already stated, the "bonded" interactions, $v_{str}(x)$, $v_{ben}(x)$, and $v_{ito}(x)$, are not included in the criterion for the acceptance probability ($\lambda_n^{(1)} = 1$ for each n). In SGE-1 and SGE-8 simulations, the dimensionless works for optimal weight calculation are recorded every 60 fs (L_a parameter introduced in point 2 of section 5), while optimal weight updates are attempted every 21 ps (L_b parameter introduced in point 3 of section 5). The parameter L_a adopted to store work samples ensures a loss of work correlation of about 50%, resulting from the autocorrelation functions of the dimensionless work reported in Figure 1S of the Supporting Information. The threshold N' (see points 3a and 3b in section 5) employed for the number of work samples in the optimal weight update is 350. In SGE and RE simulations, replica transitions are attempted every 300 fs. The system snapshots are stored every 300 fs for the subsequent data analysis. In all simulations, the total time per replica is 12 ns, so that the overall sampling time is 96 ns for the SGE-8 and RE simulations, while it is 12 ns for the SGE-1 and canonical simulations.

Table 1. Components of the Vector $\boldsymbol{\lambda}_n \equiv (\lambda_n^{(1)},\lambda_n^{(2)},\lambda_n^{(3)})$ Associated with Ensemble n for n = 1, 2, ..., 8[a]

ensemble	$\lambda_n^{(1)}$	$\lambda_n^{(2)} = \lambda_n^{(3)}$
$\boldsymbol{\lambda}_1$	1	1
$\boldsymbol{\lambda}_2$	1	0.75
$\boldsymbol{\lambda}_3$	1	0.50
$\boldsymbol{\lambda}_4$	1	0.30
$\boldsymbol{\lambda}_5$	1	0.15
$\boldsymbol{\lambda}_6$	1	0.08
$\boldsymbol{\lambda}_7$	1	0.03
$\boldsymbol{\lambda}_8$	1	0.01

[a]The vector components, $\lambda_n^{(1)}$, $\lambda_n^{(2)}$, and $\lambda_n^{(3)}$ correspond, respectively, to the $v_1^a(x)$, $v_2^a(x)$, and $v_3^a(x)$ terms of the potential energy decomposition of eq 10. The $\boldsymbol{\lambda}_1$ ensemble represents the unperturbed system.

All simulations have been performed with the 5.2 release of the ORAC program[33,34] (http://www.chim.unifi.it/orac).

7. RESULTS AND DISCUSSION

When comparing SGE to RE, we have to consider aspects which range from the possibility of sampling the λ space effectively to the capability of the methods to overcome large free energy barriers and hence to visit important configurational states of the system. Although efficient λ-space sampling is a

dx.doi.org/10.1021/ct2008457 | J. Chem. Theory Comput. 2012, 8, 830−842

requirement for any generalized ensemble method, be it of the PGE or SGE type, it does not ensure by itself the achievement of good configurational sampling. Therefore, a comparison between multiensemble methods cannot disregard a direct evaluation of their performances in exploring free energy landscapes.

Following these guidelines, we first analyze some time-dependent feature correlated with the sampling of the λ space. In this regard, we notice that, given the strong correlation between λ-space sampling and λ-dependent free energy (see discussion in section 3), the estimate of the latter could provide useful complementary information. Thus, the λ-dependent free energy is analyzed using two computational strategies, namely the *a posteriori* reweighting technique MBAR[15] (see section I of the Supporting Information) and the BAR-SGE method employed to update the λ-ensemble free energies during the SGE simulations (see section 5). Establishing the efficiency of the updating free energy algorithm is of basic importance for proving the reliability and the self-consistency of BAR-SGE based simulations. In the second part of this section, as a representative example of free energy exploration, we report on the configurational sampling of alanine dipeptide in terms of the Φ and Ψ dihedral angles (see Figure 1) by calculating the free energy surface $F(\Phi,\Psi) = -k_B T \ln[g(\Phi,\Psi)]$, where $g(\Phi,\Psi)$ is the $\Phi-\Psi$ distribution function. We also provide an estimate of the rate of overcoming a large free energy barrier occurring around $\Phi = 0°$ in the $\Phi-\Psi$ space of the alanine dipeptide.

7.1. λ-Space Sampling. The first quantity to be monitored for investigating λ-space sampling is certainly the mean acceptance probability of replica transitions between neighboring λ ensembles. The mean acceptance probabilities for the SGE-1, SGE-8, and RE simulations are reported in Table 2. Since in RE simulations replica transitions occur via exchanges of replica pairs, the numbers of upward and downward transitions between two given λ ensembles are equal. Instead, such numbers can be different in SGE simulations because each replica moves independently in the λ space. This explains why in Table 2 a single estimate is given for RE, as compared to two independent estimates for SGE. We point out that the values of acceptance probabilities of contiguous pairs of ensembles ($\boldsymbol{\lambda}_1 \rightarrow \boldsymbol{\lambda}_2$, $\boldsymbol{\lambda}_2 \rightarrow \boldsymbol{\lambda}_3$, and so on) are not supposed to follow a special pattern. In fact, the $\boldsymbol{\lambda}_n$ parameters of Table 1 have been tuned in a short RE simulation to give roughly comparable acceptance probabilities. However, some features are expected: (1) in SGE simulations, upward and downward transitions between two given λ ensembles ($\boldsymbol{\lambda}_n \rightarrow \boldsymbol{\lambda}_{n+1}$ and $\boldsymbol{\lambda}_n \leftarrow \boldsymbol{\lambda}_{n+1}$, respectively) must be accepted with equal probability in the infinite time limit; (2) this probability does not depend on the number of replicas but only on the $\boldsymbol{\lambda}_n$ and $\boldsymbol{\lambda}_{n+1}$ parameter; (3) for a given λ set, the acceptance probabilities of SGE simulations will be greater than those of RE simulations.[18,19,23] The first feature is observed in both SGE simulations, though at a different degree of accuracy. In fact, in SGE-8 simulations, the absolute differences between the mean acceptance probabilities of conjugated upward and downward replica transitions are on average 0.4%, the maximum value being 0.9% ($\boldsymbol{\lambda}_1 \rightarrow \boldsymbol{\lambda}_2$ and $\boldsymbol{\lambda}_1 \leftarrow \boldsymbol{\lambda}_2$ transitions in Table 2). Due to statistical reasons, the percentage increases to 1.3% for the SGE-1 simulation (the maximum value of 2.2% also occurs for the $\boldsymbol{\lambda}_1 \rightarrow \boldsymbol{\lambda}_2$ and $\boldsymbol{\lambda}_1 \leftarrow \boldsymbol{\lambda}_2$ transitions). In the limit of the statistical differences between SGE-1 and SGE-8, the second feature above can also be verified from the data of Table 2. The third feature is confirmed beyond any statistical uncertainty: the average difference between SGE-8 and RE mean acceptance probabilities (the former being calculated as the arithmetic average of the upward and downward values) is 16.1%, the smallest value of 15.5% occurring for the $\boldsymbol{\lambda}_5-\boldsymbol{\lambda}_6$ pair.

Table 2. Acceptance Probabilities of Replica Transitions (in Percentage) Calculated in the Whole Simulation Time (12 ns per Replica) for the SGE-1, SGE-8, and RE Simulations[a]

	SGE-1		SGE-8		RE
ensembles	→	→	→	→	⇌
$\boldsymbol{\lambda}_1, \boldsymbol{\lambda}_2$	43.1	40.9	41.3	42.2	24.8
$\boldsymbol{\lambda}_2, \boldsymbol{\lambda}_3$	38.8	38.8	37.7	38.1	22.2
$\boldsymbol{\lambda}_3, \boldsymbol{\lambda}_4$	41.4	41.3	42.3	42.8	25.5
$\boldsymbol{\lambda}_4, \boldsymbol{\lambda}_5$	40.3	38.3	38.7	38.7	22.8
$\boldsymbol{\lambda}_5, \boldsymbol{\lambda}_6$	49.9	47.9	49.5	49.0	33.8
$\boldsymbol{\lambda}_6, \boldsymbol{\lambda}_7$	40.9	38.9	38.7	39.0	23.1
$\boldsymbol{\lambda}_7, \boldsymbol{\lambda}_8$	42.8	41.8	42.6	42.9	27.0

[a]The column "ensembles" reports the ensembles involved in replica transitions, while the arrows indicate the direction of the transitions (example: the right arrow denotes transitions from $\boldsymbol{\lambda}_n$ to $\boldsymbol{\lambda}_{n+1}$).

The above results indicate that the replicas perform transitions between neighboring λ ensembles with quite large probability, pointing to an effective λ-space sampling. A more conclusive outcome for this issue can be obtained by analyzing the time series of the λ ensembles visited by each replica. Such series are drawn in Figure 2 for replicas randomly chosen from the SGE-8 and RE simulations, and for the only replica of the SGE-1 simulation. In order to highlight the oscillations and the short time behavior of the time series, we limit the data of Figure 2 to the first nanosecond. The complete sets of data for SGE-8 and RE simulations are reported in Figures 2S and 3S of the Supporting Information. Figure 2 shows that replica random walks in λ space are realized in all simulations. In spite of the larger acceptance probabilities of the SGE simulations with respect to the RE simulation (see Table 2), in the long time limit, the degree of diffusion of replicas through the λ space seems not to differ significantly among the three runs. However, at short times, the first complete walk from the bottom to the top ensemble and back requires increasingly long times in the series RE < SGE-8 < SGE-1 (from 0.1 to 0.3 ns approximately). This feature is known for the BAR-SGE methodology[26] and is ascribed to the inaccurate estimate of the optimal weights at the beginning of the simulation. Reaching the random-walking regime more or less quickly depends crucially on the rate with which accurate optimal weights are achieved that, in turn, increases with the number of running replicas. In RE simulations, λ-ensemble free energies do not enter the acceptance criterion for replica exchanges, and hence the random-walking regime is reached more quickly than in SGE runs. Nevertheless, when the whole simulation is considered, the average round-trip times between the top and bottom ensembles become comparable: 0.15 ns (RE), 0.11 ns (SGE-8), and 0.12 ns (SGE-1).

In order to assess the differences between SGE and RE methods in reaching the replica random-walking regime, we have calculated a time-dependent population function, denoted as $P_{i\alpha}(t)$, aimed to quantify the fraction of time spent by a given replica α in a given $\boldsymbol{\lambda}_i$ ensemble

$$P_{i\alpha}(t) = \frac{n_{i\alpha}(t)}{\sum_{j=1}^{N_s} n_{j\alpha}(t)} \qquad (17)$$

dx.doi.org/10.1021/ct2008457 | J. Chem. Theory Comput. 2012, 8, 830−842

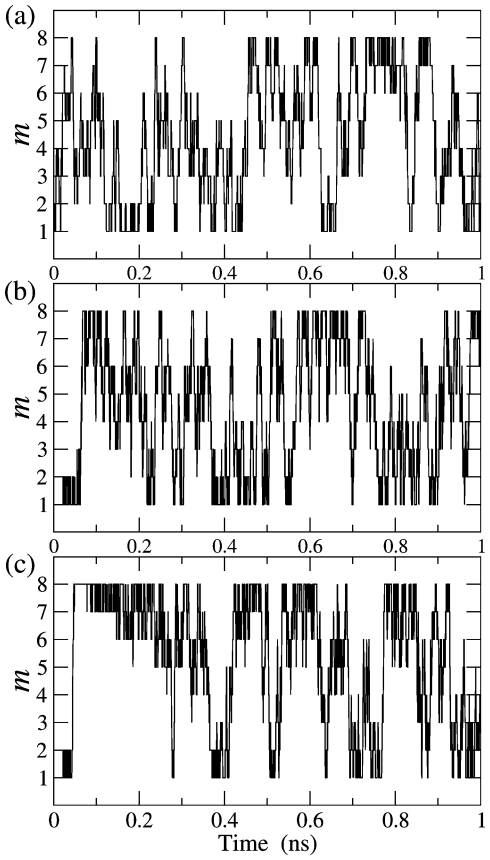

Figure 2. Time series of the m label of λ_m related to a randomly chosen replica for RE and SGE-8, and to the only one replica in SGE-1. (a) RE simulation, (b) SGE-8 simulation, and (c) SGE-1 simulation. For the sake of clarity, only the data of the first nanosecond are reported.

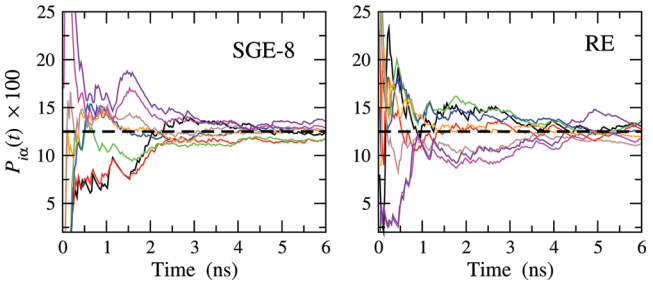

Figure 3. Population function $P_{i\alpha}(t)$ (eq 17) for two replicas randomly chosen from SGE-8 and RE simulations (left and right panels, respectively). To highlight the early time behavior, only data for half the simulation run are shown. The correspondences between colors and λ ensembles follow: black/λ_1, red/λ_2, green/λ_3, blue/λ_4, orange/λ_5, brown/λ_6, magenta/λ_7, violet/λ_8. The value corresponding to a homogeneous distribution, i.e., 12.5, is represented by the dashed lines.

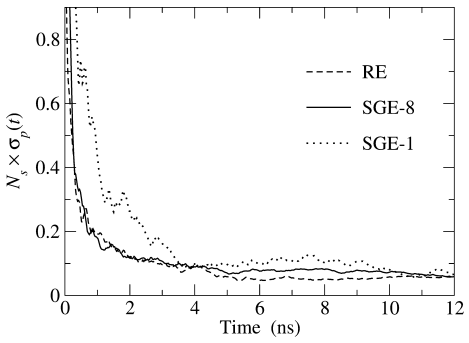

Figure 4. Variation coefficient of the root-mean-square deviation of the ensemble populations, $\sigma_p(t)/N_s^{-1}$, as a function of time (see eq 18). Dashed line, RE simulation; solid line, SGE-8 simulation; dotted line, SGE-1 simulation.

where $n_{i\alpha}(t)$ is the number of times the αth replica is found in the ensemble λ_i during the time t and N_s is the number of ensembles. Thus, for each replica, there are N_s population functions. It is evident that in the case of perfect replica random walk (as it should be, in principle, for RE and SGE simulations), each replica will spend the same amount of time in each λ ensemble, that is, $\lim_{t\to\infty} n_{i\alpha}(t) = \lim_{t\to\infty} n_{j\beta}(t)$, for any i, j, α, and β, and thus $\lim_{t\to\infty} P_{i\alpha}(t) = N_s^{-1}$. The eight population functions determined for two replicas randomly chosen from SGE-8 and RE simulations are reported in Figure 3. The complete sets of data are reported in Figures 4S and 5S of the Supporting Information. Comparing the $P_{i\alpha}(t)$ functions with their infinite time limit, $N_s^{-1} = 1/8$, we see that, after an initial period with large statistical uncertainty, convergence is going to be attained. The most important aspect is however that no significant differences are observed between RE and SGE approaches. This situation is even more evident by collecting the whole set of information of $P_{i\alpha}(t)$ in a unique quantity such as the root-mean-square deviation of all $P_{i\alpha}(t)$ functions from the theoretical value N_s^{-1}

$$\sigma_p(t) = \sqrt{(N_s N_r)^{-1} \sum_{i=1}^{N_s} \sum_{\alpha=1}^{N_r} [N_s^{-1} - P_{i\alpha}(t)]^2} \qquad (18)$$

where N_r is the number of replicas. On the basis of the preceding discussion, the infinite time limit of $\sigma_p(t)$ must be zero when the replicas realize completely random walks. The time series of the relative value (coefficient of variation) of $\sigma_p(t)$, defined as $\sigma_p(t)/N_s^{-1}$, are drawn in Figure 4. As noted above, apart from the early time behavior, SGE-8 and RE simulations give comparable trends. Below ~0.2 ns, $\sigma_p(t)$ is greater for the SGE-8 simulation probably because of the inaccurate initial estimates of optimal weights that lead to a nonuniform population of λ ensembles. The convergence rate for the SGE-1 simulation is slower than for SGE-8 and RE simulations, though above 4 ns the three $\sigma_p(t)$ curves are comparable.

7.2. λ-Ensemble Free Energies. As demonstrated in section 3, uniform sampling of λ ensembles can be obtained only when the weight factors correspond to λ-ensemble free energies. Therefore, estimating the rate of convergence of λ-ensemble free energies and, in particular, the free energy differences entering the acceptance probabilities (eq 14) is a basic test for evaluating the performances of the BAR-SGE protocol. In fact, slow convergence may not ensure an effective sampling of the λ space, thus making it difficult to overcome phase space energy barriers in a reasonable amount of computer time. In Figure 5, we report the time series of four representative dimensionless free energy differences ($\Delta f_{n\to n+1}$ with $n = 1, 3, 5, 7$), calculated with BAR-SGE during the SGE-1 and SGE-8 runs. The other free energy differences are reported in Figure 6S of the Supporting Information. We point out that such free energy differences are computed by exploiting the complete BAR-SGE procedure (point 3a of section 5), i.e., weighting each independent estimate by the inverse of its

dx.doi.org/10.1021/ct2008457 | J. Chem. Theory Comput. 2012, 8, 830–842

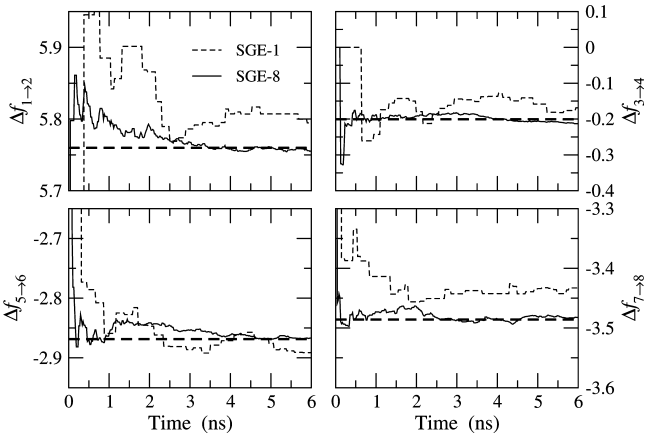

Figure 5. Time series of selected dimensionless free energy differences between neighboring λ ensembles (see y axes) calculated using BAR-SGE. Thin dashed lines, SGE-1 simulation; solid lines, SGE-8 simulation; horizontal dashed lines, reference value calculated from RE simulation using MBAR with all trajectory data (12 ns per replica). The curves are drawn until 6 ns to highlight the early time behavior.

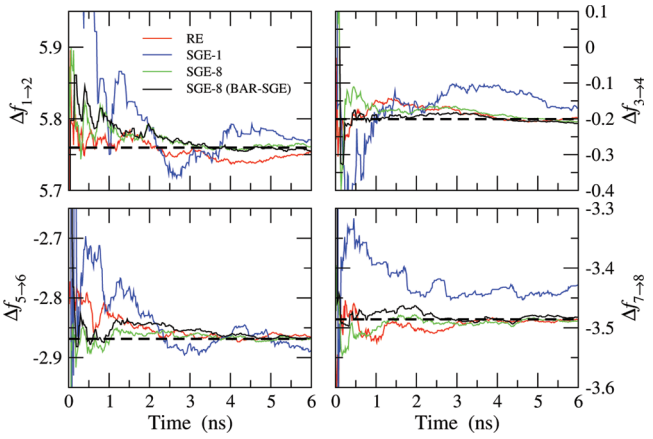

Figure 6. Time series of selected dimensionless free energy differences between neighboring λ ensembles (see y axes). Red lines, RE simulation using MBAR; blue lines, SGE-1 simulation using MBAR; green lines, SGE-8 simulation using MBAR; black lines, SGE-8 simulation using BAR-SGE (same as in Figure 5); dashed lines, reference value calculated from RE simulation using MBAR with all trajectory data (12 ns per replica). The curves are drawn until 6 ns to highlight the early time behavior.

variance as described in Appendix B. In Figure 5, we also report the reference value calculated from the RE simulation using MBAR with the complete set of data (12 ns per replica). It is noticeable that, in the SGE-8 simulation, the λ-ensemble free energy differences have almost reached convergence above ~0.2 ns. Again, the lower statistics of the SGE-1 run do not allow a convergence of comparable quality. In spite of this, the absolute values of the deviations of the free energy differences from the reference ("exact") values after 6 ns, denoted as $\delta(\Delta f_{n\to n+1})$, fall in the range 0.006−0.053. From these deviations, one can estimate the error on the ratio P_n/P_m of the probabilities of visiting the $\boldsymbol{\lambda}_n$ and $\boldsymbol{\lambda}_m$ ensembles (see eq 7). The uncertainty $\delta(\Delta f_{m\to n})$ propagates exponentially to the ratio P_n/P_m:

$$\frac{P_n}{P_m} = \frac{Z_n}{Z_m} e^{\Delta f_{m\to n} \pm \delta(\Delta f_{m\to n})} = e^{\pm\delta(\Delta f_{m\to n})} \tag{19}$$

In the case of the SGE-1 simulation, taking the largest value for $\delta(\Delta f_{m\to n})$ (0.053 at 6 ns), we obtain $P_n/P_m \approx 1 \pm 0.05$. The same estimate for the SGE-8 simulation gives a ratio in the interval 1 ± 0.02. A rough estimate of the error on the ratio between the end ensemble probabilities, P_{N_s}/P_1, can also be obtained by assuming that $\delta(\Delta f_{1\to N_s}) = \sum_{n=1}^{Ns-1}\delta(\Delta f_{n\to n+1})$. For the SGE-1 and SGE-8 simulations at 6 ns, the ratios P_{N_s}/P_1 fall in the ranges 1 ± 0.25 and 1 ± 0.04, respectively. In light of the restrictive assumptions, these results confirm the relatively good accuracy of the method.

The data of Figure 5 point to a good efficiency of BAR-SGE for achieving fast convergence of optimal weights. Further insight can be obtained from comparing the free energy differences $\Delta f_{n\to n+1}$ calculated with BAR-SGE and *a posteriori* with MBAR. Such a comparison helps in understanding two important aspects of the problem. One is the rate of convergence of BAR-SGE optimal weights (specifically, this is obtained from the comparison between BAR-SGE and RE free energy differences, the latter from MBAR), while the other is the relative efficiency of BAR-SGE with respect to the more accurate MBAR method applied on the trajectories of the SGE simulations. The time series for the four free energy differences discussed above are reported in Figure 6. The remaining sets of data are in Figure 7S of the Supporting Information. As usual, owing to poor statistics, SGE-1 and short-time SGE-8 series are affected by larger uncertainty. In some cases, above 0.2 ns both calculations for the SGE-8 simulation (BAR-SGE and MBAR) show an even faster convergence than RE. The reasons for the (sometimes) better performances of BAR-SGE with respect to RE are actually unclear and even contrary to expectations. In fact, while in MBAR all replica configurations contribute to the calculation of the λ-ensemble free energies (see section I of the Supporting Information), in BAR-SGE only data collected from neighboring λ ensembles are exploited (see eq 15). Therefore, we are inclined to consider these features as simply fortuitous. It is also worth noting that the time series calculated for the SGE simulations with BAR-SGE and MBAR have a very close trend. This is explained by the fact that in MBAR the major contribution to a given free energy difference $\Delta f_{n\to n+1}$ is given by the data collected from the $\boldsymbol{\lambda}_n$ and $\boldsymbol{\lambda}_{n+1}$ ensembles. Consistently with this fact, only these data are employed in the BAR-SGE algorithm (see eq 15).

7.3. Sampling the Φ−Ψ Conformational Space. As often remarked, the power of SGE and PGE (multiensemble) techniques is directly associated with the possibility of overcoming high free energy barriers and hence to the possibility of visiting system configurations not accessible to conventional computer simulations. This important feature is investigated here by focusing on the conformational space of the dihedral Φ and Ψ angles of alanine dipeptide (see Figure 1). Such a choice is particularly suitable for our aim because the conformational space for $-30° < \Phi < 120°$ cannot be accessed with a standard canonical simulation. This is shown in Figure 7, where we report the time series of the Φ angle values recorded during the canonical molecular dynamics simulation and during trajectories of representative replicas of the SGE-1, SGE-8, and RE simulations. Note that the setup of the canonical simulation, especially the initial configuration, is the same as that of multiensemble simulations. While conformational states with $\Phi < -30°$ are explored with all types of methods, the states

dx.doi.org/10.1021/ct2008457 | J. Chem. Theory Comput. 2012, 8, 830−842

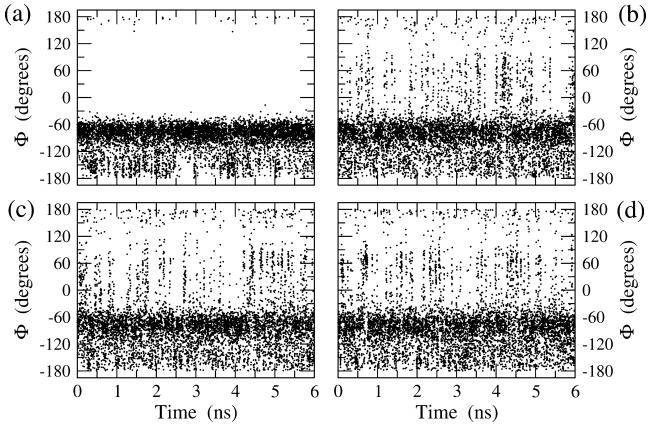

Figure 7. Time series of the Φ angle. (a) canonical simulation, (b) RE simulation, (c) SGE-1 simulation, and (d) SGE-8 simulation. In RE and SGE-8, data of one replica chosen at random are shown.

characterized by $\Phi > -30°$ are visited only with multiensemble techniques.

The effectiveness of multiensemble techniques in overcoming the free energy barrier observed at $\Phi \sim 0°$[9] may be evaluated by directly counting the number of times that alanine dipeptide realizes a conformational transition from $\Phi = -30°$ to $\Phi = 30°$ and vice versa, regardless of the Ψ value. The results, reported in Table 3, show that SGE simulations generate

Table 3. Number of Conformational Transitions $\Phi = -30° \rightleftharpoons \Phi = 30°$ Realized by the Alanine Dipeptide During the RE, SGE-1, and SGE-8 Simulations (12 ns per Replica)

replica	RE	SGE-8	SGE-1
1	346	422	436
2	338	398	
3	312	428	
4	248	388	
5	382	370	
6	386	338	
7	290	369	
8	376	344	
mean value	334.7	382.1	436
std. deviation	48.9	33.2	

more conformational transitions with respect to RE. As shown in Figure 7, no conformational transitions have been found during the canonical simulation. However, in view of the large spread of the values in the table, it is fair to say that the performances of RE and BAR-SGE are comparable.

A more detailed picture of the aspects discussed above is obtained from the free energy projection onto Φ−Ψ space, i.e., $F(\Phi,\Psi) = -k_B T \ln[g(\Phi,\Psi)]$, where $g(\Phi,\Psi)$ is the Φ−Ψ distribution function calculated by means of MBAR reweighting (see eq 7 of the Supporting Information). The free energies $F(\Phi,\Psi)$ for the canonical and multiensemble simulations are depicted in Figure 8. We note that in the range $50° < \Phi < 100°$, the free energy surface has a relative minimum with energy higher, by ∼20 kJ mol^{-1}, than that of the two absolute minima falling at $(\Phi,\Psi) \simeq (-70°, -20°)$ and $(\Phi,\Psi) \simeq (-70°, 160°)$. It is remarkable that, because of the large free energy barrier around $\Phi \sim 0°$, this minimum is revealed only with RE and SGE simulations. Figure 8 also highlights the effect of sampling on the free energy calculation (compare the free energy surfaces from RE and SGE-8 simulations to that obtained from the SGE-1 simulation). The difference between SGE-1 and SGE-8 simulations is basically due to statistical reasons, as can be proved by comparing the $F(\Phi,\Psi)$ functions calculated respectively from the whole SGE-1 simulation data (with overall sampling time of 12 ns) and from the SGE-8 simulation by limiting the time per replica to 1.5 ns (which amounts to 12 ns cumulatively). As expected, the two free energy surfaces do not show significant differences (see Figure 8S of the Supporting Information). For our aim, it is however important to observe that RE and SGE-8 simulations, having both an overall sampling time of 96 ns, give free energy surfaces that are almost indistinguishable (see Figure 8). These surfaces are comparable to those calculated with other methods,[9,31] though the free energy maxima appear overestimated. This can be ascribed to the fact that high free energy configurations are mainly sampled from replicas in low-λ ensembles, whose weights in thermodynamic averages are very small, and hence the error is large. The performances of multiensemble techniques in reproducing free energy barriers are somehow comparable to those of conventional umbrella sampling simulations,[35] in which configurations generated at high temperatures are reweighted in the low-temperature target ensemble. The inaccuracy in reweighting from low-λ ensembles is also responsible for the large error of SGE-1 in estimating the two smaller free energy barriers along the Ψ direction at about $-180° < \Phi <- 90°$, $\Psi \sim -110°$ and $-180° < \Phi < -90°$, $\Psi \sim 80°$. In this respect, note that the time spent by the SGE-1 replica in the target ensemble, i.e., λ_1, which contributes mostly to the statistics of $F(\Phi,\Psi)$, is about 1/8 the sampling time of the canonical simulation. This also explains the largely noisy behavior of the SGE-1 free energy surface with respect to the canonical counterpart.

In order to quantify the differences between the free energy surfaces of Figure 8, we resort to the analysis of the deviation of $g(\Phi,\Psi)$ from a reference Φ−Ψ distribution function. Since we are dealing with the performances of BAR-SGE in relation to the well-established RE technique, we take the distribution calculated from the latter method as the reference. In particular, we estimate

$$s(t) = \sqrt{G^{-2} \sum_{i=1}^{G} \sum_{j=1}^{G} [g_t(\Phi_i, \Psi_j) - g_{\mathrm{ref}}(\Phi_i, \Psi_j)]^2} \qquad (20)$$

where $g_{\mathrm{ref}}(\Phi_i,\Psi_j)$ is the RE reference distribution function at the point (Φ_i,Ψ_j) calculated by exploiting all stored configurations and G is the number of histogram channels employed for Φ and Ψ. The subscript t in $g_t(\Phi,\Psi)$ denotes the trajectory time considered for the calculation of the distribution function. Moreover, in eq 20, the distribution functions are both normalized, i.e.,

$$\sum_{i=1}^{G} \sum_{j=1}^{G} g_{\mathrm{ref}}(\Phi_i, \Psi_j) = \sum_{i=1}^{G} \sum_{j=1}^{G} g_t(\Phi_i, \Psi_j) = 1 \qquad (21)$$

The $s(t)$ functions for the SGE-1, SGE-8, and RE simulations are reported in Figure 9. For the RE simulation, $s(t)$ is exactly zero at 12 ns because of the assumption $g_{\mathrm{ref}}(\Phi,\Psi) = g^{\mathrm{RE}}_{12\mathrm{ns}}(\Phi,\Psi)$, with obvious meaning of the superscript and subscript. The remarkable but not surprising result is that the trends of the SGE-8 and RE $s(t)$ functions are comparable for the whole simulation time. As usual, the SGE-1 curve is less accurate because of

dx.doi.org/10.1021/ct2008457 | J. Chem. Theory Comput. 2012, 8, 830−842

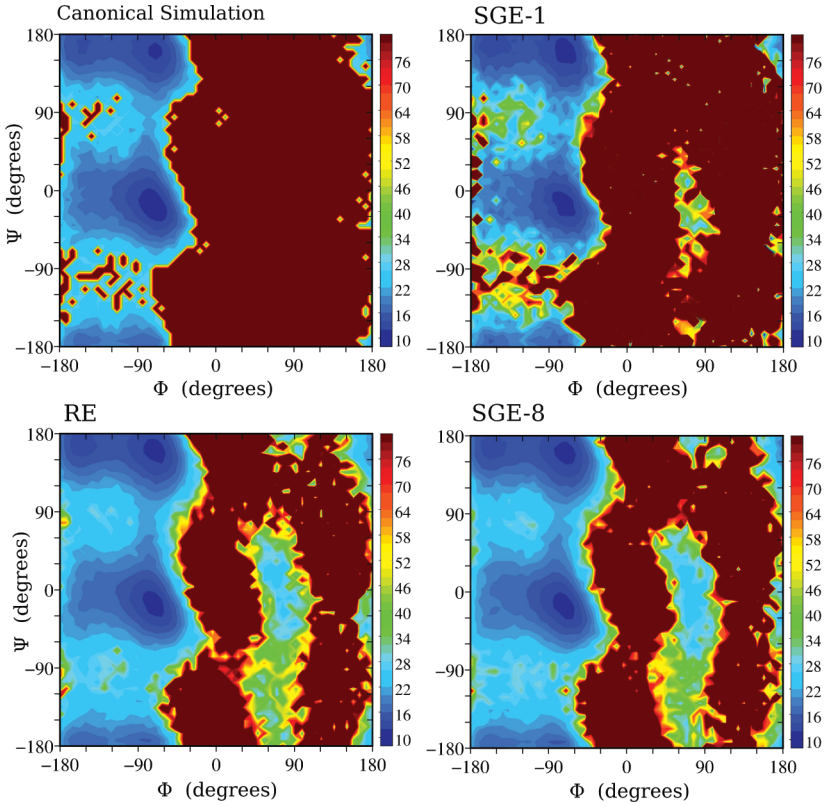

Figure 8. Φ−Ψ projection of the free energy surface, $F(\Phi,\Psi)$, calculated from the RE, SGE-8, SGE-1, and canonical simulations (see labels on top left of the panels). The chromatic scale on the right of the panels is in units of kJ mol^{-1}. The deep brown color marks regions with out of scale $F(\Phi,\Psi)$. The histogram channel size for Φ and Ψ is 7.2°.

poorer statistics. This is confirmed by comparing the final $s(t)$ value of the SGE-1 simulation to those of the SGE-8 and RE simulations calculated at 1.5 ns, namely, the time at which the overall sampling of SGE-8 and RE equals the SGE-1 one. Such values are indeed similar: $s(t) = 2.5 \times 10^{-4}$ for SGE-1, $s(t) = 3.2 \times 10^{-4}$ for SGE-8, and $s(t) = 2.7 \times 10^{-4}$ for RE.

In summary, the time series of Φ, the free energy $F(\Phi,\Psi)$, and the related data on $g(\Phi,\Psi)$ (Figures 7−9, respectively)

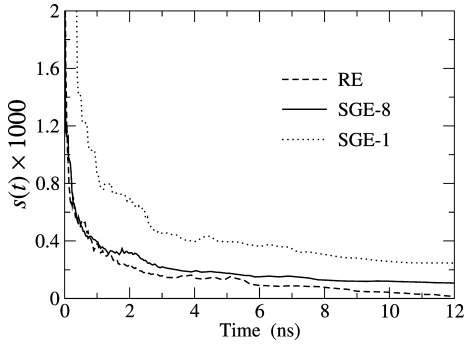

Figure 9. Time-dependence of the root-mean-square deviation of $g_t(\Phi,\Psi)$ from the reference one, $g_{ref}(\Phi,\Psi)$ (see eq 20). Dashed line, RE simulation; solid line, SGE-8 simulation; dotted line, SGE-1 simulation.

indicate a strong similarity of RE and BAR-SGE based methods in sampling the conformational space of alanine dipeptide.

8. CONCLUDING REMARKS

In simulated tempering and, more generally, in serial generalized ensemble (SGE) simulations, the weight factors entering the acceptance probability of replica transitions need to be determined somehow to obtain uniform sampling of replicas in the space of the ensembles and hence a good exploration of the free energy landscape. Uniform sampling can be achieved only if weight factors correspond to the free energies of the ensembles. In this respect, adaptive methods,[25] such as the object of the present study[26] (called BAR-SGE), provide an effective determination of weight factors without resorting to preparatory simulations.[16,21−23] This is indeed advantageous because the weight factors from preparatory simulations may not be accurate enough for ensuring uniform sampling.[11] The BAR-SGE method offers interesting perspectives in enhancing the convergence of optimal weights with minimal introduction of tunable parameters. The relevant parameter that comes into play is the frequency of updating of the weight factors during the simulation, which must ensure the storage of a sufficient number of work samples to get accurate free energy estimates (see eq 15). Although the rate of convergence of the optimal weights is quite fast for the system under study, it is obviously expected to slow down with the system size, like in all SGE-based methodologies.[16,23] Further investigation is warranted in order to assess how the convergence of thermodynamical averages scales with system size in BAR-SGE as compared to RE. The above and other issues are addressed here through the comparison of two BAR-SGE simulations with a RE simulation performed on a system made of one alanine dipeptide in water solution. The motivation of this study is two-fold. On one side, we provide a test of the BAR-SGE algorithm, which is more physically meaningful than those made on the simple model system of the original article;[26] at the same time, we furnish a thorough comparison of BAR-SGE with the more popular RE

dx.doi.org/10.1021/ct2008457 | J. Chem. Theory Comput. 2012, 8, 830−842

approach. On the other hand, we present several variants of the SGE method (simulated solute tempering, Hamiltonian simulated tempering, and multiwindow tempering), made available to the interested reader via ORAC, a free of charge program for molecular dynamics simulations (http://www.chim.unifi.it/orac).

The overall conclusion is that, by using the BAR-SGE algorithm, SGE simulations can be performed with a convergence of thermodynamic properties comparable to that observed in RE simulations at the same computational cost. Our analysis is focused on (i) the sampling of the extended-system ensembles, (ii) the convergence of the ensemble free energy differences, and (iii) the free energy surface as a function of the dipeptide dihedral angles Φ and Ψ. We have shown that BAR-SGE addresses (successfully) the most critical aspect of SGE simulations, while leaving the other features of the methodology unaltered. In view of its main advantage—not requiring synchronization and communication between replicas/processors—SGE with a BAR-SGE calculation of optimal weights is, in our opinion, a valid and attractive alternative to standard RE schemes for the simulation of complex molecular systems.

A. MULTIWINDOW TEMPERING

In MWT, the probabilities of accepting replica transitions are determined by SGE-like criteria. Any type of collective coordinate can, in principle, be adopted for sampling. Three geometrical coordinates are actually used in the ORAC program: (1) the distance between two atoms, (2) the bending angle defined by three, not necessarily bonded, atoms, and (3) the dihedral angle defined by four, not necessarily bonded, atoms. The choice of the atoms is indeed arbitrary and may not respect the molecular nature of the system. The sampling is enhanced by means of harmonic potential terms (the window potentials) acting on such geometrical coordinates, whose equilibrium values depend parametrically on $\boldsymbol{\lambda}_n = (\lambda_n^{\mathrm{dist}}, \lambda_n^{\mathrm{bend}}, \lambda_n^{\mathrm{dihed}})$. Of course, one or two components of $\boldsymbol{\lambda}_n$ can be identically zero for any $n \in (1, 2, ..., N)$. To simplify the discussion, we limit the illustration of the method to simulations where the collective coordinate corresponds to an atom−atom distance (e.g., the end-to-end distance of a polypeptide). In this case, the dimensionless Hamiltonian of a replica in ensemble n is

$$h_n(x, p) = \beta[V(x) + u(p) + k(r - \lambda_n^{\mathrm{dist}})^2] \tag{22}$$

where $V(x)$ and $u(p)$ have the usual meaning, k is a constant, and r is the instantaneous distance between the two chosen atoms. Like in SST, replica transitions are realized at fixed configurations and momenta. Thus, applying the known procedure, we recover the acceptance probability for an attempted $(x,p)_n \rightarrow (x,p)_m$ replica transition:

$$\mathrm{acc}[n \rightarrow m] = \min(1, e^{\beta k[(r-\lambda_n^{\mathrm{dist}})^2 - (r-\lambda_m^{\mathrm{dist}})^2] + \Delta f_{n\rightarrow m}}) \tag{23}$$

If additional geometrical coordinates are introduced in the definition of the collective coordinate, then the related harmonic potential terms (analogous to that of eq 22) will appear in the dimensionless Hamiltonian. Note that the constant k of the previous equations determines the stiffness of the window potentials. To obtain not negligible acceptance probabilities via large λ-ensemble overlaps, the values of k and of the differences $\lambda_{n+1}^{\mathrm{dist}} - \lambda_n^{\mathrm{dist}}$ must be chosen properly. If k is large and the differences $\lambda_{n+1}^{\mathrm{dist}} - \lambda_n^{\mathrm{dist}}$ are not small enough, then the acceptance probabilities of eq 23 will vanish. On the other hand, if k is small, then the window potentials will be very broad and therefore unable to allow for an extensive sampling of the space of the collective coordinate.

B. OPTIMAL WEIGHT EVALUATION FROM INDEPENDENT ESTIMATES AND ASSOCIATED VARIANCES

As discussed in section 5, optimal weights are evaluated basically via eq 15, and only temporary values are obtained from eq 16. For each pair of neighboring ensembles, the simulation produces a series of independent estimates of free energy differences, say $\Delta f_1, \Delta f_2, ..., \Delta f_P$ (see point 3a of section 5). Here, for convenience, the subscript in Δf_i labels independent estimates of a given pair of neighboring ensembles. The series is updated with a rate specified by the L_b parameter introduced in point 3 of section 5. Therefore, the number P of independent free energy estimates depends, on average, on the current simulation time and on L_b. For each Δf_i, it is possible to quantify the uncertainty through the associated variance $\delta^2(\Delta f_i)$ calculated following Shirts et al.:[43]

$$\begin{aligned}\delta^2(\Delta f_{n\rightarrow m}) = 2\{ &\sum_{i=1}^{N_{n\rightarrow m}} [1 + \cosh(W_i[n \rightarrow m] - \Delta f')]^{-1} \\ &+ \sum_{j=1}^{N_{m\rightarrow n}} [1 + \cosh(W_j[m \rightarrow n] + \Delta f')]^{-1}\}^{-1} \\ &- N_{n\rightarrow m}^{-1} - N_{m\rightarrow n}^{-1}\end{aligned} \tag{24}$$

where $\Delta f' = \Delta f_{n\rightarrow m} + \ln(N_{m\rightarrow n}/N_{n\rightarrow m})$ (see eq 15 for the notation). The quantity $\delta^2(\Delta f_{n\rightarrow m})$ can be calculated once $\Delta f_{n\rightarrow m}$ is recovered from eq 15. We can then write $\hat{\Delta} f$, the optimal estimator of $P^{-1}\sum_{i=1}^{P}\Delta f_i$, by a weighted sum of the individual estimates:[26]

$$\hat{\Delta} f = \frac{\sum_{i=1}^{P} [\delta^2(\Delta f_i)]^{-1} \Delta f_i}{\sum_{j=1}^{P} [\delta^2(\Delta f_j)]^{-1}} \tag{25}$$

When at least one Δf_i estimate is available, the quantity $\hat{\Delta} f$ is used as the optimal weight in the acceptance probability of eq 14.

■ ASSOCIATED CONTENT

Supporting Information

Section I: Recipes to calculate ensemble free energy differences and thermodynamical averages in SGE (and RE) simulations using the MBAR method. Equations specific for SST and MWT, as implemented in the ORAC program, are also provided. Figure 1S: Normalized autocorrelation functions of the dimensionless work as a function of time. Figures 2S and 3S: Replica walks through the $\boldsymbol{\lambda}_m$ ensembles in SGE-8 and RE simulations, respectively. Figures 4S and 5S: Population function $P_{i\alpha}(t)$ (eq 17) for the replicas of the SGE-8 and RE simulations, respectively. Figure 6S: Time series of ensemble free energy differences calculated during the SGE-1 and SGE-8 simulations by using BAR-SGE. Figure 7S: Time series of ensemble free energy differences calculated *a posteriori* for the SGE-1, SGE-8, and RE simulations by using MBAR. Figure 8S: Φ−Ψ projection of the free energy surface calculated from the SGE-8 and SGE-1 simulations using the same overall time. This information is available free of charge via the Internet at http://pubs.acs.org.

dx.doi.org/10.1021/ct2008457 | J. Chem. Theory Comput. 2012, 8, 830−842

AUTHOR INFORMATION

Corresponding Author

*E-mail: riccardo.chelli@unifi.it.

Notes

The authors declare no competing financial interest.

ACKNOWLEDGMENTS

The authors are grateful to Simone Marsili and Piero Procacci (Department of Chemistry, University of Firenze, Italy) for stimulating discussions and for technical help in the implementation of the program ORAC. This work was supported by European Union Contract RII3-CT-2003-506350.

REFERENCES

(1) Okamoto, Y. *J. Mol. Graphics Modell.* **2004**, *22*, 425.
(2) Marinari, E.; Parisi, G. *Europhys. Lett.* **1992**, *19*, 451.
(3) Lyubartsev, A. P.; Martsinovski, A. A.; Shevkunov, S. V.; Vorontsov-Velyaminov, P. N. *J. Chem. Phys.* **1992**, *96*, 1776.
(4) Hansmann, U. H. E. *Chem. Phys. Lett.* **1997**, *281*, 140.
(5) Sugita, Y.; Okamoto, Y. *Chem. Phys. Lett.* **1999**, *314*, 141.
(6) Hukushima, K.; Nemoto, K. *J. Phys. Soc. Jpn.* **1996**, *65*, 1604.
(7) Tesi, M. C.; van Rensburg, E. J. J.; Orlandini, E.; Whittington, S. G. *J. Stat. Phys.* **1996**, *82*, 155.
(8) Fukunishi, H.; Watanabe, O.; Takada, S. *J. Chem. Phys.* **2002**, *116*, 9058.
(9) Itoh, S. G.; Okumura, H.; Okamoto, Y. *J. Chem. Phys.* **2010**, *132*, 134105.
(10) Liu, P.; Kim, B.; Friesner, R. A.; Berne, B. J. *Proc. Natl. Acad. Sci. U.S.A.* **2005**, *102*, 13749.
(11) Denschlag, R.; Lingenheil, M.; Tavan, P.; Mathias, G. *J. Chem. Theory Comput.* **2009**, *5*, 2847.
(12) Li, H.; Fajer, M.; Yang, W. *J. Chem. Phys.* **2007**, *126*, 024106.
(13) Kumar, S.; Bouzida, D.; Swendsen, R. H.; Kollman, P. A.; Rosenberg, J. M. *J. Comput. Chem.* **1992**, *13*, 1011.
(14) Ferrenberg, A. M.; Swendsen, R. H. *Phys. Rev. Lett.* **1989**, *63*, 1195.
(15) Shirts, M. R.; Chodera, J. D. *J. Chem. Phys.* **2008**, *129*, 124105.
(16) Park, S.; Pande, V. S. *Phys. Rev. E* **2007**, *76*, 016703.
(17) Rauscher, S.; Neale, C.; Pomès, R. *J. Chem. Theory Comput.* **2009**, *5*, 2640.
(18) Park, S. *Phys. Rev. E* **2008**, *77*, 016709.
(19) Zhang, C.; Ma, J. *J. Chem. Phys.* **2008**, *129*, 134112.
(20) Gallicchio, E.; Levy, R. M.; Parashar, M. *J. Comput. Chem.* **2008**, *29*, 788.
(21) Hansmann, U. H. E.; Okamoto, Y. *J. Comput. Chem.* **1997**, *18*, 920.
(22) Irbäck, A.; Potthast, F. *J. Chem. Phys.* **1995**, *103*, 10298.
(23) Mitsutake, A.; Okamoto, Y. *Chem. Phys. Lett.* **2000**, *332*, 131.
(24) Huang, X.; Bowman, G. R.; Pande, V. S. *J. Chem. Phys.* **2008**, *128*, 205106.
(25) Park, S.; Ensign, D. L.; Pande, V. S. *Phys. Rev. E* **2006**, *74*, 066703.
(26) Chelli, R. *J. Chem. Theory Comput.* **2010**, *6*, 1935.
(27) Chelli, R.; Marsili, S.; Barducci, A.; Procacci, P. *Phys. Rev. E* **2007**, *75*, 050101.
(28) Chelli, R. *J. Chem. Phys.* **2009**, *130*, 054102.
(29) Bennett, C. H. *J. Comput. Phys.* **1976**, *22*, 245.
(30) Zwanzig, R. W. *J. Chem. Phys.* **1954**, *22*, 1420.
(31) Marsili, S.; Barducci, A.; Chelli, R.; Procacci, P.; Schettino, V. *J. Phys. Chem. B* **2006**, *110*, 14011.
(32) Laio, A.; Parrinello, M. *Proc. Natl. Acad. Sci. U.S.A.* **2002**, *99*, 12562.
(33) Procacci, P.; Paci, E.; Darden, T.; Marchi, M. *J. Comput. Chem.* **1997**, *18*, 1848.
(34) Marsili, S.; Signorini, G. F.; Chelli, R.; Marchi, M.; Procacci, P. *J. Comput. Chem.* **2010**, *31*, 1106.
(35) Torrie, G. M.; Valleau, J. P. *J. Comput. Phys.* **1977**, *23*, 187.
(36) Beutler, T. C.; van Gunsteren, W. F. *J. Chem. Phys.* **1994**, *100*, 1492.
(37) In Monte Carlo generalized ensemble simulations, momenta are dropped out.
(38) Mitsutake, A.; Okamoto, Y. *J. Chem. Phys.* **2009**, *130*, 214105.
(39) Here, we assume implicitly that the indexes n and m belong to an ordered list such that $T_1 < T_2 < ... < T_N$ (in simulated tempering simulations) or $\lambda_1 < \lambda_2 < ... < \lambda_N$ (in generic SGE simulations).
(40) Darden, T.; York, D.; Pedersen, L. G. *J. Chem. Phys.* **1993**, *98*, 10089.
(41) Essmann, U.; Perera, M. L.; Berkovitz, M. L.; Darden, T.; Lee, H.; Pedersen, G. L. *J. Chem. Phys.* **1995**, *103*, 8577.
(42) Frenkel, D.; Smit, B. *Understanding Molecular Simulations: From Algorithms to Applications*; Academic Press: San Diego, 2002; pp 505−507.
(43) Shirts, M. R.; Bair, E.; Hooker, G.; Pande, V. S. *Phys. Rev. Lett.* **2003**, *91*, 140601.
(44) Jarzynski, C. *Phys. Rev. Lett.* **1997**, *78*, 2690.
(45) Duan, Y.; Wu, C.; Chowdhury, S.; Lee, M. C.; Xiong, G. M.; Zhang, W.; Yang, R.; Cieplak, P.; Luo, R.; Lee, T.; Caldwell, J.; Wang, J. M.; Kollman, P. *J. Comput. Chem.* **2003**, *24*, 1999.
(46) Jorgensen, W. L.; Chandrasekhar, J.; Madura, J. D.; Impey, R. W.; Klein, M. L. *J. Chem. Phys.* **1983**, *79*, 926.
(47) Hoover, W. G. *Phys. Rev. A* **1985**, *31*, 1695.
(48) Tuckerman, M. E.; Berne, B.; Martyna, G. *J. Chem. Phys.* **1992**, *97*, 1990.